A&A 427, 987–994 (2004)
DOI: 10.1051/0004-6361:20040039

Astronomy & Astrophysics

Co-moving frame radiative transfer in spherical media with arbitrary velocity fields

E. Baron[1,2,3] and P. H. Hauschildt[4]

[1] Dept. of Physics and Astronomy, University of Oklahoma, 440 W. Brooks, Rm 131, Norman, OK 73019, USA
e-mail: baron@nhn.ou.edu
[2] Computational Research Division, Lawrence Berkeley National Laboratory, MS 50F-1650, 1 Cyclotron Rd, Berkeley, CA 94720-8139, USA
[3] Laboratoire de Physique Nucléaire et de Hautes Énergies, CNRS-IN2P3, University of Paris VII, Paris, France
[4] Hamburger Sternwarte, Gojenbergsweg 112, 21029 Hamburg, Germany
e-mail: yeti@hs.uni-hamburg.de

Received 8 January 2004 / Accepted 30 July 2004

Abstract. Recently, with the advances in computational speed and availability there has been a growth in the number and resolution of fully 3D hydrodynamical simulations. However, all of these simulations are purely hydrodynamical and there has been little attempt to include the effects of radiative transfer except in a purely phenomenological manner because the computational cost is too large even for modern supercomputers. While there has been an effort to develop 3D Monte Carlo radiative transfer codes, most of these have been for static atmospheres or have employed the Sobolev approximation, which limits their applicability to studying purely geometric effects such as macroscopic mixing. Also the computational requirements of Monte Carlo methods are such that it is difficult to couple with 3D hydrodynamics. Here, we present an algorithm for calculating 1D spherical radiative transfer in the presence of non-monotonic velocity fields in the co-moving frame. Non-monotonic velocity flows will occur in convective, and Raleigh-Taylor unstable flows, in flows with multiple shocks, and in pulsationally unstable stars such as Mira and Cepheids. This is a first step to developing fully 3D radiative transfer than can be coupled with hydrodynamics. We present the computational method and the results of some test calculations.

Key words. radiative transfer

1. Introduction

The equation of radiative transfer (RTE) in spherical symmetry for moving media has been solved with a number of different methods, e.g. Monte Carlo calculations (Magnan 1970; Caroff et al. 1972; Auer & Blerkom 1972), Sobolev methods (Castor 1970), the tangent ray method (Mihalas et al. 1976), and the DOME method (Hauschildt & Wehrse 1991). Today's state-of-the-art computer codes use iterative methods for the solution of the RTE, based on the philosophy of operator splitting or operator perturbation (Cannon 1973; Scharmer 1984). Following these ideas, different approximate Λ-operators for this "accelerated Λ-iteration" (ALI) method have been used successfully (Olson et al. 1987; Hamann 1987; Werner 1987) and have been applied to the construction of non-LTE, radiative equilibrium models of stellar atmospheres (Werner 1987). Hauschildt (1992) and Hauschildt et al. (1994) have developed an operator splitting method based on the short-characteristic method (Olson et al. 1987; Olson & Kunasz 1987) to obtain the formal solution of the special relativistic, spherically symmetric RTE along its characteristics and a band-diagonal approximation to the discretized Λ-operator. This method can be implemented very efficiently to obtain an accurate solution of the spherically symmetric RTE for continuum and line transfer problems using only modest amounts of computer resources.

The main restriction of the co-moving frame (CMF) method discussed in Hauschildt (1992) is a restriction to monotonic velocity fields. For monotonic velocity fields, the wavelength derivative part of the CMF RTE can be posed as an initial value problem with the initial conditions set at small wavelengths for expanding media and at long wavelengths for contracting media. The initial value problem has to be solved by a fully implicit wavelength discretization (e.g., upwind schemes) in order to guarantee stability. In media with non-monotonic velocity fields, the wavelength derivative changes the structure of the equation so that it becomes a boundary value problem with boundary conditions at both short and long wavelengths. Since the equation is first order in wavelength at each spatial point there is only one boundary condition, whose wavelength sense depends on the local sign of the coefficient of the derivative. Therefore, if the wavelength-space is discretized to solve the CMF RTE, we need *local* upwind schemes in order to guarantee stability and to properly account for the presence of mixed boundary conditions in wavelength-space.

In principle, it is possible to solve the RTE in the observer's frame, however, in that frame the emission and absorption processes are anisotropic and a detailed calculation is extremely complex. The main obstacle at high velocity, is that a prohibitively large number of wavelength and angle points are required to solve the observer's frame RTE.

In this paper, we describe an operator splitting method to solve the spherical relativistic CMF RTE for arbitrary velocity fields. The method can be applied to a wide variety of astrophysical problems; e.g., atmospheres of pulsating stars, stellar atmospheres with shocks, multi-component novae, and supernova atmospheres. Although we present the method for the spherically symmetric 1-dimensional case, it can be extended to 3D geometry. Our approach calculates the formal solution along each characteristic independently (for known source function) in the combined radius-wavelength space. This has to be done in order to account for the wavelength and radial boundary conditions simultaneously during the formal solution stage of the operator splitting method. As the "approximate Λ operator" we use a block matrix that is tri-diagonal in wavelength space where each spatial (i.e., radial) block is itself a band matrix. This "wavelength tri-diagonal" approach yields superior convergence compared to a simpler "wavelength diagonal" approach (which would correspond to a diagonal approximate Λ operator in static radiative transfer problems). The work presented here is a first step in an effort to develop methods for solving the CMF RTE in fully 3D geometry, but even in its spherical version presented here will be useful for studying varying stars, such as Miras and Cepheids.

2. Method

In the following discussion we use notation of Hauschildt (1992). Our starting point is the spherically symmetric form of the special relativistic, time independent ($\partial/\partial t \equiv 0$) RTE, the restriction to plane parallel geometry is straightforward. The calculation of the characteristics is identical to Hauschildt (1992) and we thus assume that the characteristics are known. First, we will describe the process for the formal solution, then we will describe how we construct the approximate Λ operator, Λ^*.

2.1. Formal solution

We begin with Eq. (16) of Hauschildt (1992) (see also Eq. (1) of Hauschildt & Baron 2004):

$$\frac{\mathrm{d}I_l}{\mathrm{d}s} + a_l \frac{\partial \lambda I}{\partial \lambda} = \eta_l - (\chi_l + 4a_l) I_l \tag{1}$$

where $\mathrm{d}s$ is a line element along a (curved) characteristic, $I_l(s)$ is the specific intensity along the characteristic at point $s \geq 0$ ($s = 0$ denotes the beginning of the characteristic) and wavelength point λ_l. The coefficient a_l is defined by

$$a_l = \gamma \left[\frac{\beta\left(1-\mu^2\right)}{r} + \gamma^2 \mu \left(\mu + \beta\right) \frac{\partial \beta}{\partial r} \right]$$

where $\beta = v/c$, $\gamma = 1/\sqrt{1-\beta^2}$ and r is the radius. η_l and χ_l are the emission and extinction coefficients at wavelength λ_l, respectively.

Equation (1) describes the change of the intensity along a arbitrary characteristic though the medium. We define

$$\hat{\chi}_l \equiv \chi_l + 4a_l$$

and discretize the wavelength derivative using a 3 point differencing formula (this can be made more general) to obtain:

$$\frac{\mathrm{d}I_l}{\mathrm{d}s} + a_l \left[p_{l,l-1} I_{l-1} + p_{l,l} I_l + p_{l,l+1} I_{l+1} \right] = \eta_l - (\chi_l + 4a_l) I_l \tag{2}$$

where $S_l = \eta_l/\chi_l$ is the source function at $\lambda = \lambda_l$, $\mathrm{d}\tau = \hat{\chi}\,\mathrm{d}s$, and the p_{ij} are the discretization coefficients for the $\partial\lambda I_l/\partial\lambda$ derivatives (see Eqs. (4) and (5) for details).

To obtain an expression for the formal solution, we rewrite Eq. (2) as

$$\frac{\mathrm{d}I_l}{\mathrm{d}\tau} = I_l - \hat{S}_l - \tilde{S}_l$$

with

$$\hat{S}_l = \frac{\chi_l}{\hat{\chi}_l} S_l = \frac{\eta_l}{\hat{\chi}_l}$$

$$\tilde{S}_l = -\frac{a_l}{\hat{\chi}_l} \left[p_{l,l-1} I_{l-1} + p_{l,l} I_l + p_{l,l+1} I_{l+1} \right]$$

(note that the index l denotes the wavelength point λ_l)

With this we obtain the following expression for the formal solution (see also Eq. (14) in Hauschildt & Baron 2004)

$$I_{i,l} = I_{i-1,l} \exp(-\Delta\tau_{i-1}) + \delta\hat{I}_{i,l} + \delta\tilde{I}_{i,l} \tag{3}$$

with the definitions

$$\delta\hat{I}_{i,l} = \alpha_{i,l}\hat{S}_{i-1,l} + \beta_{i,l}\hat{S}_{i,l} + \gamma_{i,l}\hat{S}_{i+1,l}$$

and

$$\delta\tilde{I}_{i,l} = \alpha_{i,l}\tilde{S}_{i-1,l} + \beta_{i,l}\tilde{S}_{i,l}.$$

The index i labels the (spatial) points along a characteristic, the index l denotes the wavelength point. The coefficients $\alpha_{i,l}$, $\beta_{i,l}$, and $\gamma_{i,l}$ are given in Hauschildt (1992) and Olson & Kunasz (1987), here they are calculated for a fixed wavelength for all points along a characteristic. $\hat{S}$ is a vector of known quantities (the old mean intensities and thermal sources). The $\tilde{S}$ contain the effects of the velocity field on the formal solution and are given by

$$\tilde{S}_{i-1,l} = -\frac{a_{i-1,l}}{\hat{\chi}_{i-1,l}} \left[p_{l,l-1} I_{i-1,l-1} + p_{l,l} I_{i-1,l} + p_{l,l+1} I_{i-1,l+1} \right]$$

$$\tilde{S}_{i,l} = -\frac{a_{i,l}}{\hat{\chi}_{i,l}} \left[p_{l,l-1} I_{i,l-1} + p_{l,l} I_{i,l} + p_{l,l+1} I_{i,l+1} \right].$$

This term provides the coupling of different wavelengths in the formal solution. Note that we have only used linear interpolation of the $\tilde{S}$ terms and that this differencing scheme is different than that of Hauschildt (1992). We have described this differencing scheme in detail in Hauschildt & Baron (2004). We have found that this differencing scheme is less diffusive in the co-moving frame and thus produces better line profiles

for the case of small differential expansion. It gives identical results in the case of large global differential expansion (novae and supernovae) where the numerical diffusion in the co-moving frame is overwhelmed by the global line width. We have shown that this differencing scheme can become unstable under certain conditions, but can be stabilized in a straightforward manner (Hauschildt & Baron 2004). We present here the more complex $\zeta = 1.0$, the generalization of the differencing scheme to the fully stable differencing scheme is obvious and can be found in Hauschildt & Baron (2004).

If the velocity field is monotonically increasing or decreasing, then $p_{l,l+1} \equiv 0$ or $p_{l,l-1} \equiv 0$ for a stable upwind discretization of the wavelength derivative. In these cases, the problem becomes an initial value problem and can be solved for each wavelength once the results of the previous (smaller or longer) wavelength points are known. For non-monotonic velocity fields this is no longer the case and the formal solution needs to explicitly account for the wavelength couplings in both the blue and red directions.

The formal solution is equivalent to the solution of one linear system for each characteristic. The rank of the system is $n_l \times n_i$ where n_l is the number of wavelength points and n_i is the number of points along the characteristic. For n_r radial points, we have $3 \le n_i \le 2n_r - 1$ points along each characteristic. The number of wavelength points n_l can be much larger, $n_l \approx 1000$ for the test cases presented later in this paper but $n_l \approx 300\,000$ in full scale applications, so the rank of the systems can become large. Fortunately, the linear systems have a simple structure that allows us to use efficient methods for their numerical solution.

For the construction of the system matrix for the formal solution along each characteristic it is useful to write the coefficients $k_{i,l}$ of the intensities as follows:

$$
\begin{aligned}
I_{i-1,l-1} : k_{i-1,l-1} &= -\frac{\alpha_{i,l} a_{i-1,l} p_{l,l-1}}{\hat{\chi}_{i-1,l}} \\
I_{i-1,l} : \quad k_{i-1,l} &= \exp(-\Delta\tau_{i-1}) \\
I_{i-1,l+1} : k_{i-1,l+1} &= -\frac{\alpha_{i,l} a_{i-1,l} p_{l,l+1}}{\hat{\chi}_{i-1,l}} \\
I_{i,l-1} : \quad k_{i,l-1} &= -\frac{\beta_{i,l} a_{i,l} p_{l,l-1}}{\hat{\chi}_{i,l}} \\
I_{i,l} : \quad k_{i,l} &= -\frac{\beta_{i,l} a_{i,l} p_{l,l}}{\hat{\chi}_{i,l}} \\
I_{i,l+1} : \quad k_{i,l+1} &= -\frac{\beta_{i,l} a_{i,l} p_{l,l+1}}{\hat{\chi}_{i,l}} \\
I_{i+1,l-1} : k_{i+1,l-1} &= -\frac{\gamma_{i,l} a_{i+1,l} p_{l,l-1}}{\hat{\chi}_{i+1,l}} \\
I_{i+1,l+1} : k_{i+1,l+1} &= -\frac{\gamma_{i,l} a_{i+1,l} p_{l,l+1}}{\hat{\chi}_{i+1,l}}.
\end{aligned}
$$

These expressions show the relatively simple matrix structure that can be exploited to solve for the mean intensities.

2.1.1. Discretization of $\partial\lambda I/\partial\lambda$

In order to ensure numerical stability, we use a local upwind scheme to discretize the wavelength derivative in the RTE:

- For $a_l \ge 0$:

$$\left.\frac{\partial \lambda I}{\partial \lambda}\right|_l = \frac{\lambda_l I_l - \lambda_{l-1} I_{l-1}}{\lambda_l - \lambda_{l-1}}. \tag{4}$$

- For $a_l < 0$:

$$\left.\frac{\partial \lambda I}{\partial \lambda}\right|_l = \frac{\lambda_l I_l - \lambda_{l+1} I_{l+1}}{\lambda_l - \lambda_{l+1}}. \tag{5}$$

Here, and in the following, we use a sorted wavelength grid with $\lambda_{l-1} < \lambda_l < \lambda_{l+1}$. The wavelength derivative is evaluated at a fixed spatial point along the characteristic. The coefficients p are then given by

- For $a_l \ge 0$:

$$
\begin{aligned}
p_{l,l-1} &= -\frac{\lambda_{l-1}}{\lambda_l - \lambda_{l-1}} \\
p_{l,l} &= \frac{\lambda_l}{\lambda_l - \lambda_{l-1}} \\
p_{l,l+1} &= 0.
\end{aligned}
$$

- For $a_l < 0$:

$$
\begin{aligned}
p_{l,l-1} &= 0 \\
p_{l,l} &= \frac{\lambda_l}{\lambda_l - \lambda_{l+1}} \\
p_{l,l+1} &= -\frac{\lambda_{l+1}}{\lambda_l - \lambda_{l+1}}.
\end{aligned}
$$

These coefficients depend on both the radial coordinate (because a_l is a function of r) and on the wavelengths (in the general case of a wavelength grid with variable resolution). Note that the *direction* of flow of information is determined by the sign of the coefficient a_l and not just on the velocity gradient.

2.1.2. Boundary conditions

The spatial boundary conditions in the non-monotonic case remain the same as in the monotonic case, the incoming intensities at the spatial boundaries of each characteristic must be prescribed at every *wavelength* point.

The wavelength boundary conditions are a bit more complicated, since now at every spatial point there is a wavelength boundary condition which must be determined by the local flow of information which is determined by the sign of each a_l along the characteristic. I.e., at each spatial point, one must determine whether information is flowing from blue-to-red or red-to-blue (in wavelength) and implement the proper boundary condition.

2.1.3. Structure of the system matrix

We label the total number of wavelength points n_l, and the number of intersection points along a characteristic (see Hauschildt et al. 1994) with n_i. The total number of intensities that need

to be determined is thus $n_i \times n_l$ per characteristic. Note that n_i depends on the characteristic that is used in spherical symmetry and in the general 3D case. There are two different ways to write the vector $\boldsymbol{I}$ of the specific intensities:

1. "i-ordering": $\boldsymbol{I} = (\boldsymbol{I_i})_l$, so that $\boldsymbol{I}$ is a vector of n_l vectors each of which has n_i components.
2. "l-ordering": $\boldsymbol{I} = (\boldsymbol{I_l})_i$, so that $\boldsymbol{I}$ is a vector of n_i vectors each of which has n_l components.

The position of the element (i, l) is therefore:

1. "i-ordering": $I_{il} = (l-1)n_i + i$ and
2. "l-ordering": $I_{li} = (i-1)n_l + l$.

In the following, we will denote these "block-vectors" with (n_i, n_l) for both ordering schemes.

If we write Eq. (3) in matrix form, we obtain

$$\boldsymbol{I} = A\boldsymbol{I} + \hat{S} + \tilde{S}$$

where $\hat{S}$ is a (n_i, n_l) vector with the thermal and scattering source functions for each wavelength point n_l and radial point n_i functions for each wavelength point, $\tilde{S}$ is a (n_i, n_l) vector with the wavelength derivative information, and A is a $(n_i, n_l) \times (n_i, n_l)$ matrix. The row (i, l) of A has the following entries (the location of the element for i-ordering is also given):

location	index	matrix element
$(i-1, l-1)$	$(l-2)n_i + i - 1$	$k_{i-1,l-1}$
$(i-1, l+1)$	$ln_i + i - 1$	$k_{i-1,l+1}$
$(i, l-1)$	$(l-2)n_i + i$	$k_{i,l-1}$
$(i-1, l)$	$(l-1)n_i + i - 1$	$k_{i-1,l}$
(i, l)	$(l-1)n_i + i$	$k_{i,l}$
$(i, l+1)$	$ln_i + i$	$k_{i,l+1}$
$(i+1, l-1)$	$(l-2)n_i + i + 1$	$k_{i+1,l-1}$
$(i+1, l+1)$	$ln_i + i + 1$	$k_{i+1,l+1}$.

The total bandwidth of A in the i-ordering scheme is $ln_i + i + 1 - ((l-2)n_i + i - 1) = 2(n_i + 1)$. The l-ordering scheme is symmetric to the i-ordering, thus the bandwidth in l-ordering is simply $2(n_l + 1)$. For large n_l, i-ordering will require much smaller bandwidth, therefore, we consider only the i-ordering scheme here.

To calculate the intensities along each characteristic we have to solve the linear system

$$(1 - A)\boldsymbol{I} = \hat{S} + \tilde{S} \tag{6}$$

for each characteristic where I is the identity matrix. In the i-ordering scheme, the system matrix $\mathcal{A} = I - A$ is thus a block-tridiagonal matrix with n_l blocks of $n_i \times n_i$ matrices. Figure 1 shows the general structure of the matrix $\mathcal{A}$. The $l-1$ and $l+1$ blocks are tridiagonal matrices, the l-block has the layout shown in Fig. 2. Note the sub-diagonal in the l-block is just $-\exp(-\Delta\tau_{i-1})$. For the static case, the system degenerates to one with just the l-block non-zero allowing for direct recursive solution of the problem. For monotonic velocity fields either the $l-1$ or the $l+1$ blocks are zero, again admitting recursive solution. In the case of non-monotonic velocity fields, all blocks may be non-zero and the system must be solved explicitly. It is convenient to call the tridiagonal matrix labeled $l+1$ in Fig. 1 *super*, the lower diagonal matrix labeled l, *diag*, and the tridiagonal matrix labeled $l-1$, *sub*. Then we can refer to e.g., the lower diagonal, diagonal, and upper diagonal of *super* as $A^{\rm super}$, $B^{\rm super}$, and $C^{\rm super}$, respectively.

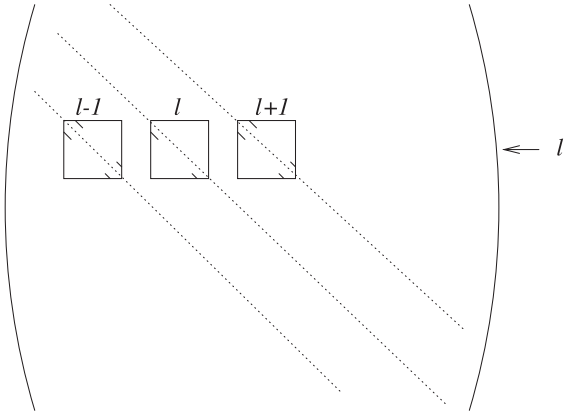

Fig. 1. Structure of the system matrix.

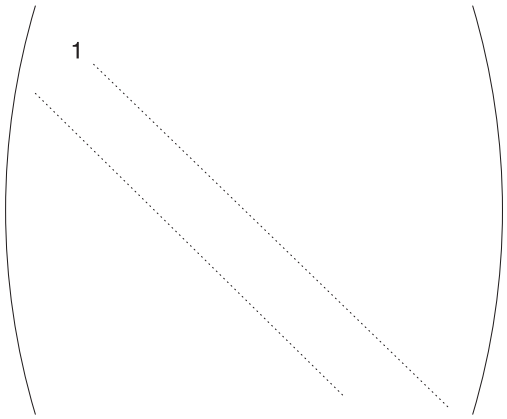

Fig. 2. Structure of the l block.

2.1.4. Solution of the linear systems

The linear system of Eq. (6) has a relatively simple structure and can be solved directly, e.g., by block tri-diagonal system solvers as described in Golub & Loan (1989). The problem with this approach is that the inverse of a tri-diagonal matrix is, in general, a *full* matrix. Therefore, the CPU time and memory requirements for direct solvers increase dramatically with increasing n_l. The special form of Eq. (6) and the sparseness of the blocks within the matrix A led us to investigate iterative methods for the solution of Eq. (6). We examined the use of the "Rapido" algorithm (Zurmühl & Falk 1986, p. 194ff), however, as with all iterative linear system solvers, the eigenvalues of the matrix can (and are in many cases) be such that this method fails. For this work we also used standard band matrix solvers available in LAPACK and ESSL, which have the advantage that the pivots only have to be calculated once per ALO iteration. Finally we used the general sparse solver package SuperLU (Xiaoye & Demmel 2003) which leads to large speedups over the other linear systems solvers we have tried (see below for a discussion of timing).

2.2. Construction of Λ^*

The major difference between the monotonic velocity field problem and the non-monotonic velocity field is that we now have to construct a combined spatial-wavelength approximate Λ operator for use in the operator splitting scheme. The basic equations of the operator splitting method remain unchanged, however. In the discussion of the construction of Λ^* it is useful to consider the "spatial" part of the Λ matrix and the "wavelength" part of the Λ matrix. The spatial part of the Λ matrix describes the transfer of photons in the radial coordinate and is, essentially, identical to the monotonic velocity field problem. The wavelength part of the Λ matrix describes the transport of photons in wavelength space due to the velocity field (or other non-coherent scattering processes).

The Λ operator at wavelength point l, Λ_l, has contributions from *all* wavelength points. This would lead to a matrix of order $n_l \times n_r$, where n_r denotes the number of radial points. With a band-matrix form for the spatial Λ^*'s, this would lead to a global band-matrix with significant storage requirements. Therefore, we derive a tri-diagonal approximation to the wavelength contributions to the global Λ^* matrix.

The construction of the *spatial* part of Λ^* proceeds in exactly the same way as described in Hauschildt et al. (1994), that is we assume a pulse of intensity of value unity is inserted into the characteristic and by acting the Λ matrix on the pulse we are able to construct and approximate lambda operator (ALO Olson et al. 1987; Olson & Kunasz 1987). Even though we have made use of the fact that the formal solution can be written as a tridiagonal operator we shall show that each component of the ALO contains effects of both spatial and wavelength propagation of the global Λ matrix.

We describe the construction of Λ^* for arbitrary (spatial) bandwidth using the example of a tangential ray (core intersecting rays are a simple specialization of this case): The intersection points (including the point of tangency) are labeled from left to right, the direction in which the formal solution proceeds. For convenience, we label the ray tangent to shell $i+1$ as i. Therefore, the ray i has $2i+1$ points of intersection with discrete shells $1 \ldots i+1$. For each point k along the ray there is a "mirror point" $k_\mathrm{m} = 2i+1-k$. To compute row j of the discrete Λ-operator (or Λ-matrix), Λ_{ij}, we sequentially label the intersection points of the ray i with the shell j ("running index"), and define auxiliary quantities $\xi^i_{k,l}$. The pulse is inserted at point k_s, which is either $k-1$ or point $k=0$ in the case $j=1$. It is convenient to define an X-factor as follows:

$$X = \begin{cases} \frac{\chi_{k_\mathrm{s},l}}{\hat{\chi}_{k_\mathrm{s},l}} \beta_{k_\mathrm{s},l} & \text{if } k = 0 \\ \frac{\chi_{k_\mathrm{s},l}}{\hat{\chi}_{k_\mathrm{s},l}} \gamma_{k_\mathrm{s},l} & \text{if } k > 0. \end{cases}$$

Then

$$\xi^i_{k_\mathrm{s},l} = \frac{X}{1 - B^\mathrm{diag}_{k_\mathrm{s},l}}$$

$$\xi^i_{k_\mathrm{s},l-1} = \frac{B^\mathrm{super}_{k_\mathrm{s},l-1} \xi^i_{k_\mathrm{s},l}}{1 - B^\mathrm{diag}_{k_\mathrm{s},l-1}}$$

$$\xi^i_{k_\mathrm{s},l+1} = \frac{B^\mathrm{sub}_{k_\mathrm{s},l+1} \xi^i_{k_\mathrm{s},l}}{1 - B^\mathrm{diag}_{k_\mathrm{s},l+1}}.$$

Then, propagating the pulse through the grid we obtain

$$X_j = \begin{cases} \frac{\chi_{j,l}}{\hat{\chi}_{j,l}} \beta_{j,l} & \text{if } j = k \\ \frac{\chi_{j,l}}{\hat{\chi}_{j,l}} \alpha_{j,l} & \text{if } j = k+1 \\ X_j + \frac{\chi_{j,l}}{\hat{\chi}_{j,l}} \gamma_{j,l} & \text{if } j = k_\mathrm{m} - 1 \\ \frac{\chi_{j,l}}{\hat{\chi}_{j,l}} \beta_{j,l} & \text{if } j = k_\mathrm{m} \\ \frac{\chi_{j,l}}{\hat{\chi}_{j,l}} \alpha_{j,l} & \text{if } j = k_\mathrm{m} + 1. \end{cases}$$

Then for $a_{j,l} < 0$ we have

$$\xi^i_{j,l+1} = \left(1 - B^\mathrm{diag}_{j,l+1}\right)^{-1} \left[A^\mathrm{sub}_{j,l+1} \xi^i_{j-1,l} + A^\mathrm{diag}_{j-1,l+1} \xi^i_{j-1,l+1}\right]$$

$$\xi^i_{j,l} = \left(1 - B^\mathrm{diag}_{j,l}\right)^{-1} \left[X + A^\mathrm{sub}_{j,l} \xi^i_{j-1,l-1} + A^\mathrm{diag}_{j,l} \xi^i_{j-1,l} + A^\mathrm{super}_{j,l} \xi^i_{j-1,l+1} + B^\mathrm{super}_{j,l} \xi^i_{j,l+1}\right]$$

$$\xi^i_{j,l-1} = \left(1 - B^\mathrm{diag}_{j,l-1}\right)^{-1} \left[A^\mathrm{diag}_{j,l-1} \xi^i_{j-1,l-1} + A^\mathrm{super}_{j,l-1} \xi^i_{j-1,l} + B^\mathrm{super}_{j,l-1} \xi^i_{j,l}\right]$$

and for $a_{j,l} \geq 0$ we have

$$\xi^i_{j,l-1} = \left(1 - B^\mathrm{diag}_{j,l-1}\right)^{-1} \left[A^\mathrm{diag}_{j,l-1} \xi^i_{j-1,l-1} + A^\mathrm{super}_{j,l-1} \xi^i_{j-1,l}\right]$$

$$\xi^i_{j,l} = \left(1 - B^\mathrm{diag}_{j,l}\right)^{-1} \left[X + A^\mathrm{sub}_{j,l} \xi^i_{j-1,l-1} + A^\mathrm{diag}_{j,l} \xi^i_{j-1,l} + A^\mathrm{super}_{j,l} \xi^i_{j-1,l+1} + B^\mathrm{super}_{j,l} \xi^i_{j,l+1}\right]$$

$$\xi^i_{j,l+1} = \left(1 - B^\mathrm{diag}_{j,l+1}\right)^{-1} \left[A^\mathrm{sub}_{j,l+1} \xi^i_{j-1,l} + A^\mathrm{diag}_{j-1,l+1} \xi^i_{j-1,l+1} + B^\mathrm{sub}_{j,l+1} \xi^i_{j,l}\right].$$

With this we can construct Λ^*'s with the full spatial bandwidth and tridiagonal in wavelength. However, in order to obtain good convergence, we also have to include wavelength dependent information in the global (spatial plus wavelength) Λ^*.

We can write the l component of the formal solution $\bar{J}_\mathrm{fs}$ in the form

$$(\bar{J}_\mathrm{fs})_l = (\Lambda S)_l \approx \Lambda_{l,l-1} S_{l-1} + \Lambda_{l,l} S_l + \Lambda_{l,l+1} S_{l+1}. \quad (7)$$

Here, $\Lambda_{l,l-1}$, $\Lambda_{l,l}$, and $\Lambda_{l,l+1}$ are the contributions to the Λ operator at wavelength point l originating from the wavelength points $l-1$, l, and $l+1$. These matrices can be computed directly from the $\lambda^i_{j,l}$ calculated above, simply by integrating over angle. Equation (7) shows explicitly the dependence of the mean intensities on the source functions of the neighboring wavelength points. Therefore, we can construct a global Λ^* operator with the definition

$$(\Lambda^* S)_l \equiv \Lambda^*_{l,l-1} S_{l-1} + \Lambda^*_{l,l} S_l + \Lambda^*_{l,l+1} S_{l+1}.$$

This leads to a block tri-diagonal global Λ^*, where each spatial block is again a band matrix with the band-width given by the full spatial Λ^*. This system can be solved efficiently either by direct solvers, using the same methods as discussed above for the formal solution. The convergence of the operator splitting method using the above Λ^* is similar to that of static operator splitting methods with a (spatial) tri-diagonal ALO. Typically, 15–20 operator splitting iterations are required to reach an accuracy of 10^{-8} for test cases with about 1000 wavelength points (see below). A wavelength-diagonal operator converges much more slowly, and an operator that ignores the wavelength dependence would require a maximum of $n_l \times n_\mathrm{iter}$ iterations where n_iter is the number of iterations required to solve a monotonic velocity field problem for a single wavelength.

3. Application examples

As a first step we have implemented the method as a serial Fortran 95 program. This allows us to test the approach on problems with a relatively small number of wavelength points. Figure 3 describes the steps involved in calculating the solution. Our basic test problem is similar to that discussed in Hauschildt (1992) and in Hauschildt & Baron (2004). We use a spherical shell with a grey continuum opacity parameterized by a power law in the continuum optical depth $\tau_{\rm std}$. The basic model parameters are

1. Inner radius $r_{\rm c} = 10^{13}$ cm, outer radius $r_{\rm out} = 10^{15}$ cm.
2. Minimum optical depth in the continuum $\tau_{\rm std}^{\rm min} = 10^{-4}$ and maximum optical depth in the continuum $\tau_{\rm std}^{\rm max} = 10^{4}$.
3. Grey temperature structure with $T_{\rm eff} = 10^4$ K.
4. Outer boundary condition $I_{\rm bc}^{-} \equiv 0$ and diffusion inner boundary condition for all wavelengths.
5. Continuum extinction $\chi_{\rm c} = C/r^2$, with the constant C fixed by the radius and optical depth grids.
6. Parameterized coherent & isotropic continuum scattering by defining

   $$\chi_{\rm c} = \epsilon_{\rm c}\kappa_{\rm c} + (1 - \epsilon_{\rm c})\sigma_{\rm c}$$

   with $0 \le \epsilon_{\rm c} \le 1$. $\kappa_{\rm c}$ and $\sigma_{\rm c}$ are the continuum absorption and scattering coefficients.
7. A parameterized spectral line with a rest wavelength of $\lambda_0 = 1000$ Å and an intrinsic width of 0.1 Å (equivalent to a width of 30 km s^{-1}), the line strength is parameterized by the ratio $\chi_{\rm l}(\lambda_0)/\chi_{\rm c}$, where $\chi_{\rm l}$ is the line extinction coefficient.
8. Parameterized line scattering defined analogous to the continuum scattering with a parameter $\epsilon_{\rm l}$. We assume complete redistribution for the line scattering.

3.1. Tests for static and monotonic velocity fields

This series of tests is designed to verify the correct operation of the code in the monotonic velocity case where we can compare it directly to our existing working code.

The monotonic velocity field tests assume a linear velocity law of the form

$$\beta(r) = \beta_0 \left(\frac{r}{r_{\rm out}} \right).$$

Where $\beta_0 = v_0/c$ is the velocity at $r_{\rm out}$.

Figure 4 displays the flux transformed to the observer's frame for a linear velocity law defined above with $v_0 = 1000$ km s^{-1}. The result is identical that produced by the purely monotonic code to the accuracy of our models. (We require that the scattering problem be solved to a relative accuracy of 10^{-8}.) We have also examined the moments in the co-moving frame and they too are identical to that obtained by the purely monotonic code. Thus, the formal solution and ALO solver and produce correct results in the regimes where we can test them directly.

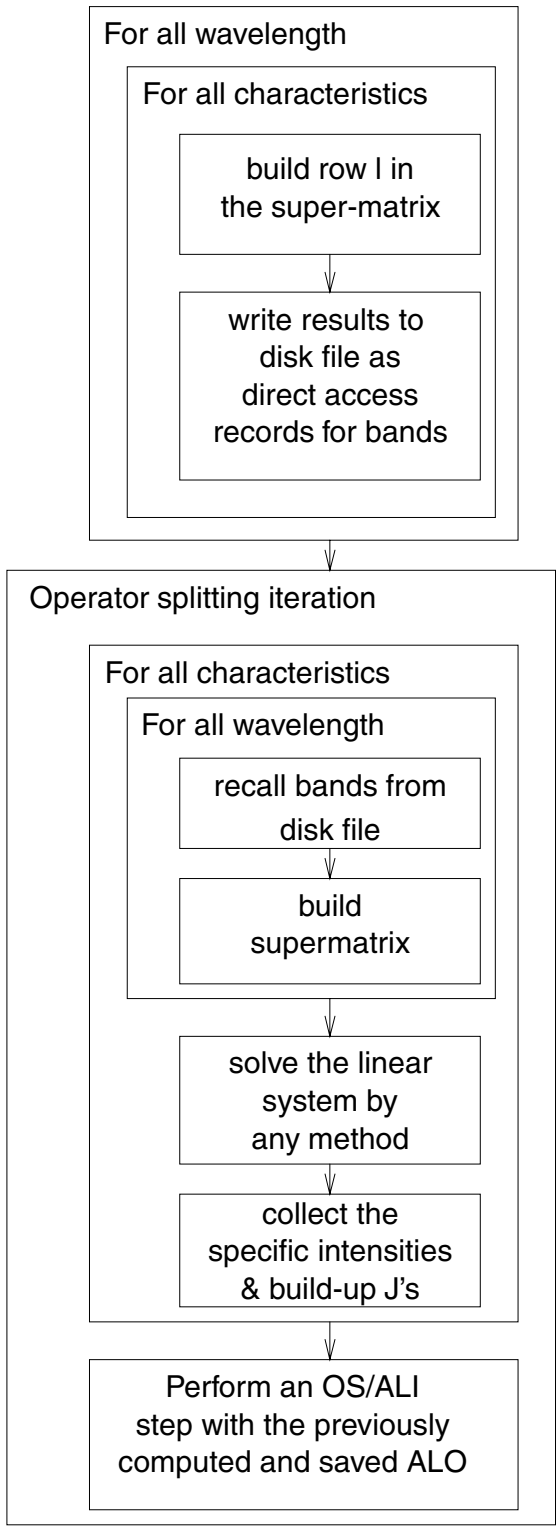

Fig. 3. Flowchart for the formal solution process.

Table 1 shows the relative time for four different matrix solvers: 99% of the time is spent in solving the linear system in the formal solution, thus the effect of varying the matrix solvers is directly related to the code speed. Interestingly, SuperLU with the matrix stored in standard LAPACK band form is slower than LAPACK, where the matrix factors are saved to disk and recalled as needed; load and store is slower

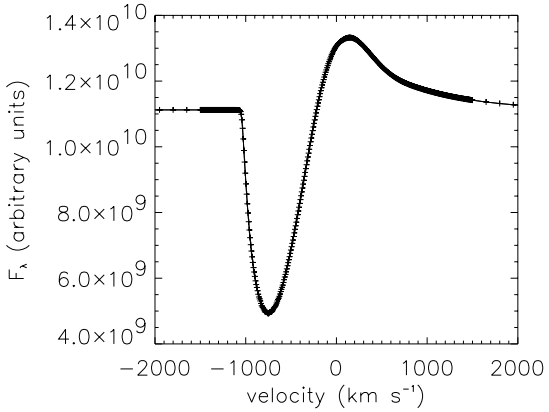

Fig. 4. The line profile in the observer's frame of the homologously expanding (linear velocity law) model. The line is the results from the monotonic velocity code (Hauschildt 1992; Hauschildt & Baron 2004) and the points are the results from the non-monotonic code for the case for $\epsilon_c = 0.1$ and $\epsilon_l = 10^{-4}$. The results are identical.

Table 1. The relative wall-clock time for a homology test with different matrix solvers. SuperLU with efficient storage leads significant speedup.

Matrix Solver	Time
LAPACK simple	740 s
LAPACK with recall	468 s
SuperLU inefficient storage	545 s
SuperLU efficient storage	178 s

than I/O! In the recall case, along a given characteristic the ALO matrix is fixed and thus once it has been factored it need not be factored again, however there are too many factors to store in memory, since the problem size is larger than available memory, particularly when scaled to real problems requiring 300 000 wavelength points. Thus, the factors must be written to disk and read into the appropriate arrays as each characteristic is solved for.

A large speedup comes from storing the SuperLU vector directly with no non-zero elements stored, even though this involves a considerable number of "if" statements in the construction loop. SuperLU can be called in a recall mode where the factors are stored similar to the LAPACK routines, but we expect to obtain much higher speedup by moving to SuperLU_DIST, the parallelized version of SuperLU and that will be discussed in a future paper.

3.2. Non-monotonic velocity fields

In order to test our algorithm we have assumed the velocity structures shown in Figs. 5 and 6. The first is a sine wave in zone number, such a structure could occur in a Mira or Cepheid variable star. The sine has been exponentially damped to mimic the effects of photon viscosity, which should strongly damp the oscillations as the material becomes optically thin (Mihalas & Mihalas 1984). The second, is just a illustrative set of piecewise continuous linear velocities, that might occur in e.g., the internal shock model of gamma-ray bursts. Figure 7 shows the

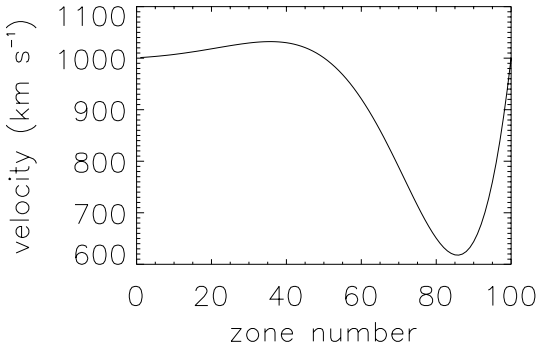

Fig. 5. The velocity profile of the sin wave model. The exponential damping accounts for the damping effects of photon viscosity.

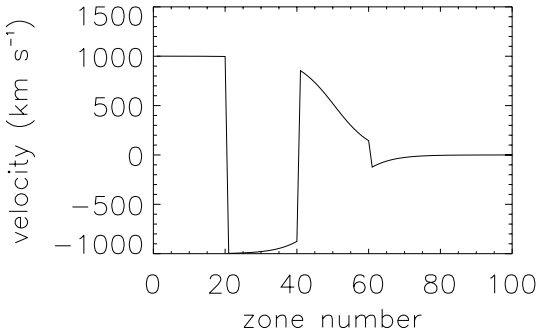

Fig. 6. The velocity profile of the "shock" model.

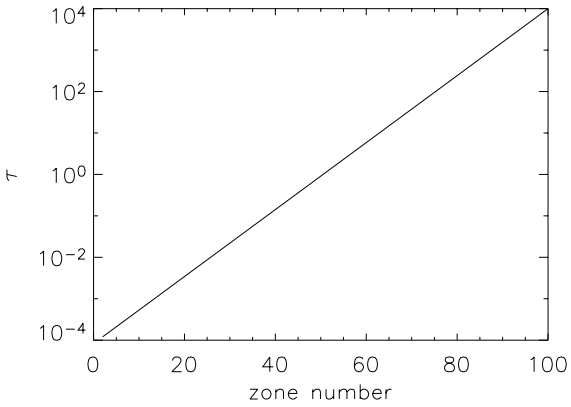

Fig. 7. The continuum optical depth as a function of zone number for comparision. The optical depth scale is the same for both the sin wave model and the "shock" model.

continuum optical depth as a function of zone number for comparison.

Figure 8 displays the observer's frame flux from the sine wave model for three choices of (ϵ_c, ϵ_l). The top panel is pure absorption in both the line and continuum, the middle panel has a pure absorptive line in a scattering continuum, and the bottom panel has a strongly scattering line in a scattering continuum. At first glance the line profile seems remarkably similar to the homologous, linear velocity law, except that there is a small dip near zero velocity. As scattering increases, the effect of the non-monotonic velocity law decreases.

Figure 9 displays the observer's frame flux from the shock wave model with the same choices for (ϵ_c, ϵ_l) as in the sine wave model. The line profile is interesting, with only a small

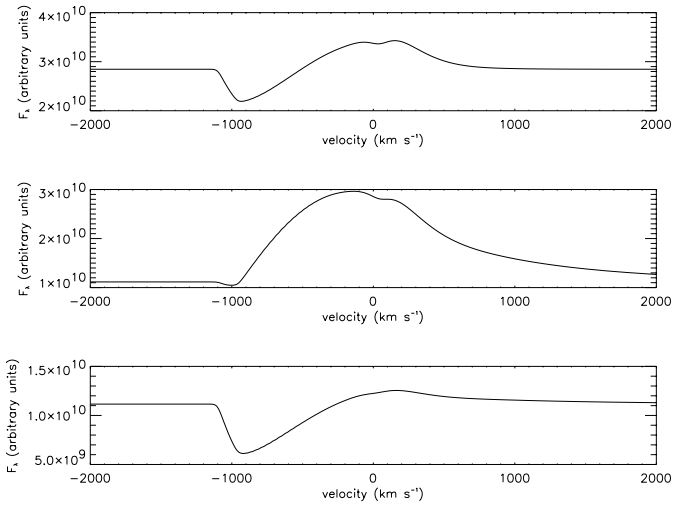

Fig. 8. The line profile in the observer's frame of the sin wave model. The top panel is for the case $\epsilon_c = \epsilon_l = 1$, the middle panel for $\epsilon_c = 0.1$ and $\epsilon_l = 1$, and the bottom panel for $\epsilon_c = 0.1$ and $\epsilon_l = 10^{-4}$.

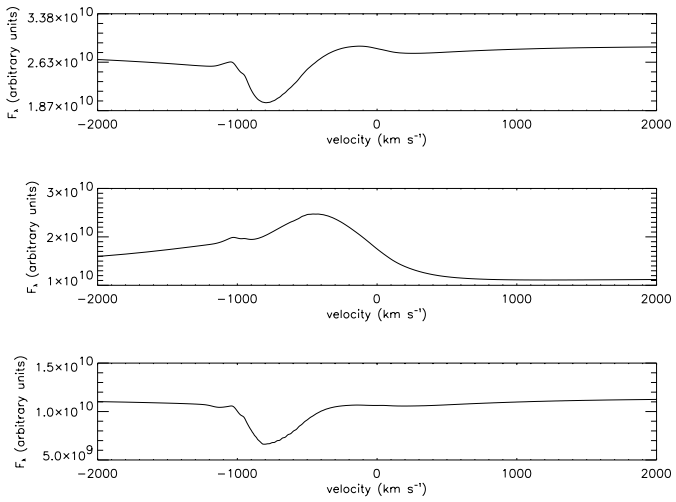

Fig. 9. The line profile in the observer's frame of the "shock" model. The top panel is for the case $\epsilon_c = \epsilon_l = 1$, the middle panel for $\epsilon_c = 0.1$ and $\epsilon_l = 1$, and the bottom panel for $\epsilon_c = 0.1$ and $\epsilon_l = 10^{-4}$.

ripple in the flux profile at negative velocity. Surprisingly, this ripple does not seem to be washed out by scattering and hence is a feature of the velocity flow.

In both cases (sine and shock) there are weak features that could be misidentified as real weak features if only homologous flows were considered.

4. Conclusions

We have presented a characteristics method of solving the full boundary value problem that occurs in both the wavelength and spatial dimension, using a full approximate lambda operator in space, and tridiagonal in wavelength. The convergence of the operator is slow for the wavelength-diagonal operator, much improved for the wavelength-tridiagonal operator. Most of the computation time is spent in solving the linear system in the formal solution. This can be both sped-up and parallelized using e.g., the SuperLU package (Xiaoye & Demmel 2003). The method we have presented is immediately useful for studying variable stars, and can be extended to 3D radiation hydrodynamics and to studying other non-coherent scattering processes such as partial redistribution, Compton scattering and neutrino transport in Raleigh-Taylor unstable flows that occur in core collapse supernovae.

Acknowledgements. We thank Sherry Xiaoye for helpful tutelage in the use of Super_LU. This work was supported in part by by NASA grant NAG5-3505, NSF grants AST-0204771 and AST-0307323, an IBM SUR grant to the University of Oklahoma and by NASA grants NAG 5-8425 and NAG 5-3619 to the University of Georgia. P.H.H. was supported in part by the Pôle Scientifique de Modélisation Numérique at ENS-Lyon. Some of the calculations presented here were performed at the San Diego Supercomputer Center (SDSC), supported by the NSF, at the National Energy Research Supercomputer Center (NERSC), supported by the US. DOE, and at the Höchstleistungs Rechenzentrum Nord (HLRN). We thank all these institutions for a generous allocation of computer time.

References

Auer, L. H., & Blerkom, D. V. 1972, ApJ, 178, 175
Cannon, C. J. 1973, JQSRT, 13, 627
Caroff, L. J., Noerdlinger, P. D., & Scargle, J. D. 1972, ApJ, 176, 439
Castor, J. I. 1970, MNRAS, 149, 111
Golub, G. H., & Loan, C. V. 1989, Matrix computations (Baltimore: Johns Hopkins University Press)
Hamann, W.-R. 1987, in Numerical Radiative Transfer, ed. W. Kalkofen (Cambridge: Cambridge Univ. Press), 35
Hauschildt, P. H. 1992, JQSRT, 47, 433
Hauschildt, P. H., & Baron, E. 2004, A&A, 417, 317
Hauschildt, P. H., & Wehrse, R. 1991, JQSRT, 46, 81
Hauschildt, P. H., Störzer, H., & Baron, E. 1994, JQSRT, 51, 875
Kalkofen, W., ed. 1987 (Cambridge: Cambridge Univ. Press)
Magnan, C. 1970, JQSRT, 10, 1
Mihalas, D., & Mihalas, B. W. 1984, Foundations of Radiation Hydrodynamics (Oxford: Oxford University)
Mihalas, D., Kunasz, P., & Hummer, D. 1976, ApJ, 206, 515
Olson, G. L., & Kunasz, P. B. 1987, JQSRT, 38, 325
Olson, G. L., Auer, L. H., & Buchler, J. R. 1987, JQSRT, 38, 431
Scharmer, G. B. 1984, in Methods in Radiative Transfer, ed. W. Kalkofen (Cambridge: Cambridge Univ. Press), 173
Werner, K. 1987, in Numerical Radiative Transfer, ed. W. Kalkofen (Cambridge: Cambridge Univ. Press), 67
Xiaoye, S. L., & Demmel, J. W. 2003, AM Transaction on Mathematical Software, 29, 110
Zurmühl, R., & Falk, S. 1986, Matrizen und ihre Anwendungen, 5th ed., Vol. 2 (Berlin: Springer-Verlag)